Peer-reviewed version available at *Journal of Sensors and Sensor Systems* **2020**, *9*, 189-197; doi:10.5194/jsss-9-189-2020

Comparison of different fiber coatings for distributed strain measurement in cementitious matrices

Martin Weisbrich*† Klaus Holschemacher† Thomas Bier‡

The distributed fiber optic strain measurement based on Rayleigh scattering has recently become increasingly popular in automotive or mechanical engineering for strain monitoring and in the construction industry, especially structural health monitoring. This technology enables the monitoring of strain along the entire fiber length. This article addresses integrating optical fibers of different coatings into the concrete matrix to measure the shrinkage deformations. However, previous studies do not give a clear statement about the strain transfer losses of fiber optic sensors in this application. In this context, three different coating types were investigated regarding their strain transfer. The fibers were integrated into fine-grained concrete prisms, and the shrinkage strain was compared with a precise dial gauge. The analysis shows a high correlation between the reference method and the fiber measurement, especially with the ORMOCER® coating. The used acrylate coating is also consistent in the middle area of the specimen but requires a certain strain introduction length to indicate the actual strain. The main result of this study is a recommendation for fiber coatings for shrinkage measurement in fine-grain concretes using the distributed fiber optic strain measurement. In addition, the advantages and disadvantages of the measurement method are presented.

1 Introduction

The development of fiber optic sensors (FOS), primarily distributed measurement methods, has led to exciting application scenarios in recent years [7, 20, 28, 32].

*Corresponding author, email: martin.weisbrich@htwk-leipzig.de
†Structural Concrete Institute, Leipzig University of Applied Science (HTWK Leipzig), Leipzig, 04275, Germany
‡Institute of Ceramics, Glass and Construction Materials, Technical University Freiberg, Freiberg, 09599, Germany

In particular, research groups published various applications for structural health monitoring (SHM) in civil engineering [3, 5, 21, 26]. The measurement methods based on Rayleigh, Brillouin, and Raman scatterings are suitable for the measurement tasks in SHM because of their distributed measurement principle. While Raman scattering only measures temperatures, Brillouin and Rayleigh scatterings can measure the temperature and strain [26]. The difference between these two methods can be found in spatial resolution, maximum measuring length, and accuracy. Using Brillouin scattering, measurement tasks of several kilometers can be realized with a spatial resolution in the centimeter range [22, 28, 30]. Rayleigh scattering used in this study has a maximum measuring length of approximately 70 m and a spatial resolution of a few millimeters [29].

The distributed fiber optic strain measurement offers essential benefits compared to established measurement methods such as fiber Bragg grating sensors (FBG), strain gauges, or inductive displacement transducers. In addition to their corrosion resistance, they are dielectric and immune to electromagnetic radiation [29]. Any point of the entire glass fiber can be used as the measuring range for the strain measurement and is not restricted to a pre-defined section [36]. Another advantage is the possibility of integrating the fiber into the building material matrix. This enables one to determine strain within concrete components, which can contain information on the curing and load behavior. Especially with massive concrete structures such as foundations or concrete roads, a strain measurement in the matrix can represent the structural and loading conditions. In prefabricated elements, the quality management of posttreatment and health monitoring can be combined. However, information on the deformation within the matrix can also lead to new design approaches in the shrinkage, creep, or swelling behavior of concrete components in research.

For a realistic representation of the strain in the matrix using fiber optic sensors, the investigation of the strain transfer from the substrate to the fiber is a primary factor (Figure 1 b). The strain is determined only in the fiber core (Figure 1 a). Two mechanisms have a decisive effect on the deformations of the fiber sensors: First, slippage can occur between the fiber cladding, so-called coating, and surrounding substrate. Second, depending on the coating material, the cladding cannot wholly transfer the strain from the substrate to the fiber cladding and the core. The model by Cheng et al. was modified in this respect and is shown in Figure 1 b [6]. The slip relationship between the substrate and the fiber coating largely depends on the curing state of the concrete. Only when the concrete has sufficiently hardened, the strain transfer can occur. The bond between coating material and concrete is critical for the strain transfer. For the slip between the fiber coating and the fiber cladding, the stiffness of the coating material is decisive for adequate transfer [4, 34, 35].

Various research groups have analyzed the effect of the fiber coating on strain transfer during measurements in the matrix. For example, Zeng et al. could determine with the help of Brillouin scattering that fiber cables showed lower strain values in the matrix than the reference method [37]. Li Quingin et al. investigated the strain transfer rates of embedded FBG sensors in mortar prisms [25]. Using a calculation

Preprints (www.preprints.org) | NOT PEER-REVIEWED | Posted: 5 March 2020 doi:10.20944/preprints201911.0046.v2

Peer-reviewed version available at Journal of Sensors and Sensor Systems 2020, 9, 189-197; doi:10.5194/jsss-9-189-2020

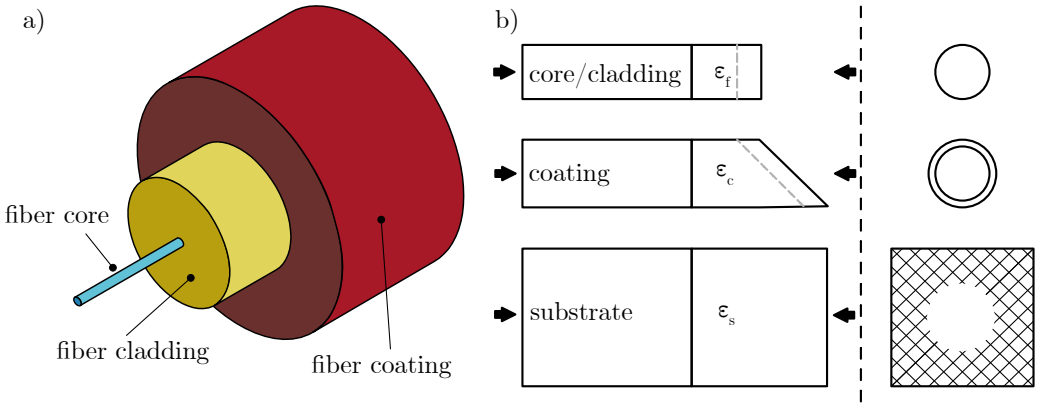

Figure 1: a) Structure of a fiber; b) Slip relationship between the matrix and the fiber core based on [6]

model, the group transferred the lower strain transfer rates (approx. 0.7-0.85) of coating material to the reference measurement level. In 2003, the research group extended its model to include pressure loads [24]. Delephine-Lesoille et al. validated a developed fiber cable and integrated it into concrete cylinders subjected to compression and tension [9]. Compared to Li Quingin et al., they achieved transfer rates of almost 100% but only in the range up to approximately $-350\,\mu\varepsilon$. Henault et al. also used fiber cables in 2010 to measure the strain in the concrete matrix [18]. In 2012, the research group investigated another type of cable [17]. In contrast to the previously presented study, the sensors showed an approximately 20% lower strain value, so a calculation model for adjustment followed [16]. In 2009, Li et al. examined various strain transfer models for different materials and confirmed them by experiments with sensors bonded to the surfaces [23]. For concrete with a modulus of elasticity of 40000 $\mathrm{N\,mm^{-2}}$, the researchers determined transfer rates of approximately 90%. In this study, experiments on the application in the concrete matrix are missing. Her et al. using a test program and an FE analysis to established a transfer function, with which the raw data consisting of high strain losses can be converted into the real strain [19]. Ohno et al. integrated fiber optic sensors into the compression and tensile zones of a concrete slab and checked the displayed strains [27]. They found that the fiber could not sufficiently anchor in the concrete structure. In [2] Bao et al. using pulse pre-pump Brillouin optical time-domain analysis to measure the shrinkage induced strain of a cylindrical mortar sample. Their investigation revealed no strain losses between the fiber measurement and the reference method. However, the precise specification about the coating used is missing. In addition, they investigated no other coating materials. Bao et al. extended their examination about the measurement of strain in the concrete matrix using DFOS: In [1] the research group detected the shrinkage-induced delamination of concrete overlays. They used two different fiber types with a coating diameter of 432 µm and 1312 µm. Despite the thick coating, the researchers do not provide any information on the strain losses or compare them

to a reference measurement. Davis et al. investigated in [8] the shrinkage-induced strains on a concrete specimen using the DFOS. The researchers bonded the fiber to a reinforcing bar, which they subsequently embedded in the concrete. Compared to the other studies, the authors used rebar as a carrier material. The strain behavior of the fiber directly in the matrix was not examined. Using a brass frame and fiber with a single layer polyimide coating, researchers around Speck fixed a fiber in small-format concrete specimens and achieved similar values to the reference measurement [31]. In the compression test, the fiber sensors revealed higher values than the strain gauge measurements on the surface.

The presented publications give contradictory statements about the strain transmission performance of optical fibers for measuring strain in the concrete matrix. In some cases, the specification of the coating used was completely omitted. Furthermore, in some investigations, the strain losses at lower loads were considerably higher than those in the tests. This article wants to make a clear statement on the strain transmission performance of optical fibers under shrinkage induced load. Therefore, the study compares the effect of three different coating materials on the strain measurement of the distributed fiber optic sensors (DFOS) in the concrete matrix. Thus, shrinkage tests on fine-grained concrete prisms are used to describe the strain behavior.

2 Experimental program

2.1 Coating materials and concrete mixture

The strain transfer properties of three different coating materials were investigated by using shrinkage tests. With two conventional coatings acrylate and polyimide, the results from the literature should be verified and form a baseline for comparison [13, 19, 25, 31]. The third coating material ORMOCER® was developed especially for FBG sensors and showed good strain transfer properties in previous investigations with bonded sensors [12, 35]. Table 1 summarizes the fiber types and their most important characteristics.

Table 1: Coating materials and fiber specifications

Coating material	Acrylate	Polyimide	ORMOCER®
Fibertype	SMF-28e+®	FSG-A01	LAL-1550-125
∅ Coating [µm]	242±5	155±5	195
∅ Cladding [µm]	125±0.7	125	125±1
Attenuation [dB km^{-1}]	< 0.02	< 0.6	< 2.5
Manufacturer	CORNING®	FBGS	FBGS

The matrix was a high-strength concrete with a maximum grain size of 2 mm, an elasticity modulus of 45 000 N mm^{-2} and a compressive strength of 111 N mm^{-2}.

Preprints (www.preprints.org) | NOT PEER-REVIEWED | Posted: 5 March 2020 doi:10.20944/preprints201911.0046.v2

Peer-reviewed version available at Journal of Sensors and Sensor Systems 2020, 9, 189-197; doi:10.5194/jsss-9-189-2020

DYCKERHOFF cement was provided as a compound [11]; all other components are listed in Table 2. The fine-grained concrete was selected according to its high shrinkage tendency, which results in a correspondingly high load on the fiber.

Table 2: Concrete mixture for the shrinkage tests based on [11]

Matrix	Unit	Quantity
BMK-D5-1 (Compound)		815
BCS 0.06/0.2		340
Sand 0/2	$[\mathrm{kg\,m^{-3}}]$	965
Water		190
Superplasticizer (MC-VP-16-0205-02)		17

2.2 Specimens and preparation

Concrete prisms with dimensions of b/h/l of 40 mm, 40 mm and 160 mm were used as the test specimen geometry. Three test specimens were produced per fiber type, which results in a test matrix of nine test specimens (Table 3). To integrate the fiber into the matrix, a modified formwork was used (Figure 2 a), where the sensors were clamped and cleaned with isopropanol. Immediately after concreting, the fiber was additionally tensioned to ensure the correct position in the specimen. A Teflon tube was used to minimize the risk of fiber breakage in the outlet areas and protruded 10 mm into the concrete matrix on each end-face (Figure 3). The area protected by the tube was not included in the analysis and is marked accordingly in Figures 5 and 6. Furthermore, the area with the Teflon tube was used for temperature compensation.

Table 3: Specimen assignment and coating material for the shrinkage tests

Nr.	Assignment	Coating material	l_0 in [mm]
1	A-1-t_i	Acrylate	160,0
2	A-2-t_i		160,1
3	A-3-t_i		160,0
4	P-1-t_i	Polyimide	159,9
5	P-2-t_i		159,9
6	P-3-t_i		160,2
7	O-1-t_i	ORMOCER®	159,9
8	O-2-t_i		160,0
9	O-3-t_i		160,4

For the reference measurement method, special measuring pins have been glued in the middle of the end-faces (Figure 4). In this regard, the fiber was arranged by

Preprints (www.preprints.org) | NOT PEER-REVIEWED | Posted: 5 March 2020 doi:10.20944/preprints201911.0046.v2

Peer-reviewed version available at Journal of Sensors and Sensor Systems 2020, 9, 189-197; doi:10.5194/jsss-9-189-2020

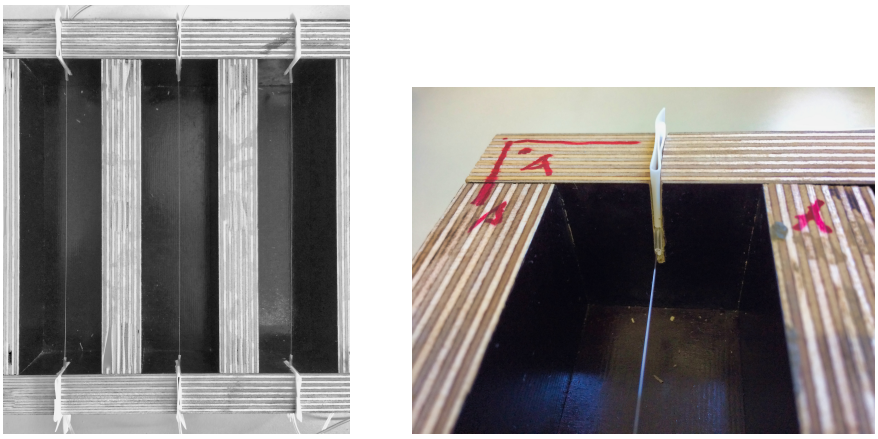

(a) (b)

Figure 2: a) Test specimen formwork with tensioned fiber; b) Fixed fiber with Teflon tube

an offset dimension of $e = 7\,\text{mm}$. The null length l_0, which is required to determine the reference strain, corresponds to the specimen length. Table 3 summarizes the zero-length, specimen designation, and associated coating materials.

2.3 Test arrangement and procedure

The test setup and procedure are based on the German standard DIN 52450 and are shown in Figure 3 [10]. At 24 hours after concreting, the test specimens were prepared for the strain measurement, which proceeded as follows:

- Stripping the test specimens
- Measuring temperature on the concrete surface with an infrared thermometer to evaluate temperature effects
- Applying the measuring pins and determining the null length l_0
- Clamping the specimens in the measuring frame (Figure 4 b)
- Reading the reference value t_0 for both measuring methods

During the experiment, the specimens were stored in a climatic box with constant climatic conditions (39% RH, 22 °C). Due to the relatively low humidity, the shrinkage load should be increased. Besides a temperature measurement of the climatic box, temperature measurement of the sample surface was also used. Due to the low deviation to the ambient temperature, the temperature effect on the strain measurement is classified as low. The strain was measured using both measuring methods after 4 and 8 days after concreting. The measurement times are listed in Table 4.

Table 4: Test times of the shrinkage tests

Time of measurement		Time after concreting [h]	[d]
	t_0	24 ±1	1
	t_1	96 ±1	4
	t_2	192 ±1	8

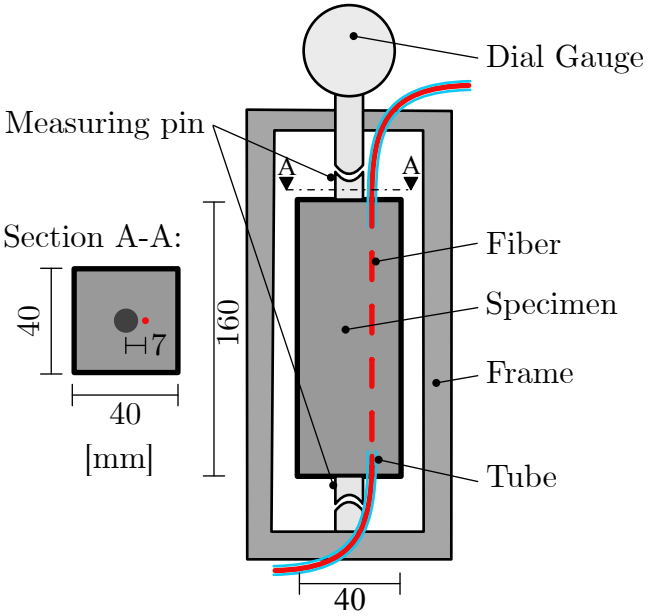

Figure 3: Arrangement of the test specimen and test setup

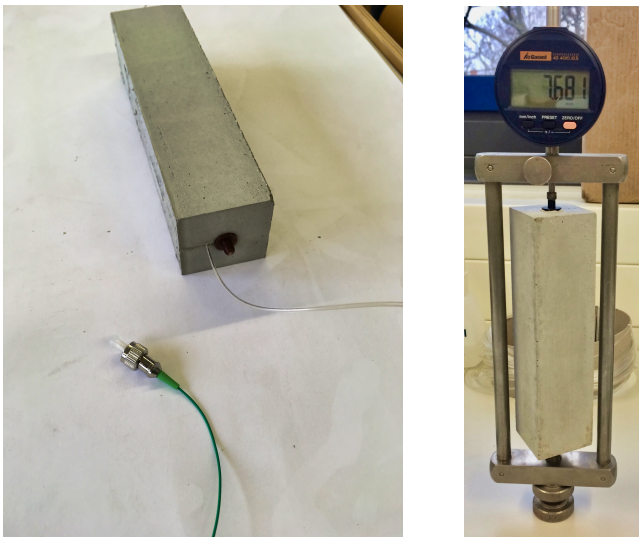

(a) (b)

Figure 4: a) Test specimen with sensor fiber and measuring pin; b) Test specimen in the measuring frame

2.4 DOFS system and reference measurement

The strain measurement of the fiber sensors was performed with the interrogator ODiSi-B from Luna Inc. The interrogator measures the Rayleigh backscattering and uses coherent frequency domain reflectometry to determine the location of the strain along the fiber. Through the frequency shift between the unloaded reference state and the loaded state and a subsequent fast Fourier transformation (FFT), the deformations can be determined. Further information on the measurement procedure can be found in the literature [14, 15, 29, 36].

Sensitive digital dial gauges were used as a reference method to measure the length change between the two measuring pins (Figures 3 and 4). The display of the difference is approximately 1/1000 mm; the error limit is 0.0005 mm.

2.5 Evaluation process

The fiber optic measurement method with its distributed measurement generates a considerable amount of data [35]: The method records a strain value for every 2.56 mm of the measuring fiber. To minimize the effect of the measurement noise, the strain values were recorded at a measuring rate of 1 Hz for 30 s at each measurement time t_i (Table 4). With a measuring length of 160 mm, 1860 strain values are recorded in the measuring range at each measurement time.

A Python-based post-process was programmed to prepare the measurement raw data accordingly. As the first step, the relevant measuring range is delimited, which results in a matrix X with approximately 62×30 measured values per sample and

Peer-reviewed version available at Journal of Sensors and Sensor Systems 2020, 9, 189-197; doi:10.5194/jsss-9-189-2020

time of measurement.

$$X_{i,t_i} = \begin{pmatrix} \varepsilon_{t_{i,1,1}} & \cdots & \varepsilon_{t_{i,1,n}} \\ \vdots & \ddots & \vdots \\ \varepsilon_{t_{i,n,1}} & \cdots & \varepsilon_{t_{i,n,n}} \end{pmatrix} \tag{1}$$

Akima interpolation [33] filters System-related measurement errors based on extreme strain variations. The authors achieved better approximations compared to other interpolation or filter methods.

To reduce the measurement noise and improve the comparability with the reference method, the matrix of equation 1 is combined using a median to form a vector with the strain values:

$$\widetilde{x_{i,t_i}} = \left[\widetilde{\varepsilon_{t_{i,1}}} \cdots \widetilde{\varepsilon_{t_{i,n}}}\right] \tag{2}$$

Figures 5 and 6 show the individual vectors of the respective specimens. Then, the average strain values and standard deviation in the comparison range can be calculated. The results of the comparison range averaging are shown in Table 5; the mean values of the specimens are shown in Table 6.

3 Results

The primary purpose of the experiments was to investigate the distributed fiber optic measurement method regarding the strain measurement in the concrete matrix. To this end, the shrinkage behavior of nine test specimens with different coating materials was investigated.

An overview of the results of the experiments is shown in Table 5. It contains the mean strain values of the fiber measurement in the comparison range, their associated standard deviation along the fiber, and the respective reference measurement at time points t_1 and t_2. The strain of the reference measurement results from the reference length l_0 (cf. Table 3) and measured value:

$$\varepsilon_r = \frac{\Delta_l}{l_0} \tag{3}$$

The mean values of the three specimens per fiber coating are shown in Table 6, and those of the reference measurement are shown in Table 7. The comparison of the two measurement methods can be characterized by the quotient between fiber measurement ε_f and reference measurement ε_r:

$$q = \frac{\varepsilon_f}{\varepsilon_r} \tag{4}$$

Figures 5 and 6 show the course of the strain along the fiber for all specimens at t_1 and t_2. The x-axis represents the fiber position, while the y-axis illustrates the

Table 5: Strain values and standard deviation in the comparison area of the fiber measurement compared to the strain values of the reference measurement at test times t_1 und t_2 in [με]

		Fiber Measurement				Reference Measurement	
		Average strain		Standard deviation			
Coating	Nr.	t_1	t_2	t_1	t_2	t_1	t_2
Acrylate	1	-583	-682	15	11	-594	-737
	2	-552	-662	26	28	-606	-737
	3	-523	-628	20	22	-581	-725
Polyimide	1	-580	-677	17	18	-613	-750
	2	-600	-710	14	14	-594	-732
	3	-549	-652	7	9	-587	-730
ORMOCER®	1	-569	-682	20	19	-563	-707
	2	-585	-702	11	13	-588	-706
	3	-549	-662	23	25	-586	-723

Table 6: Average strain values and standard deviation in the comparison area at test times t_1 und t_2 in [με]

	Strain		Standard deviation	
Coating	t_1	t_2	t_1	t_2
Acrylate	-553	-657	20	21
Polyimide	-576	-680	13	14
ORMOCER®	-568	-682	18	19

Table 7: Average strain values of the reference measurement [με]

Coating	t_1	t_2
Acrylate	-594	-733
Polyimide	-598	-738
ORMOCER®	-579	-712

Table 8: Mean strain quotients in the comparison area at test times t_1 und t_2

Coating	t_1	t_2
Acrylate	0.93	0,90
Polyimide	0.96	0,92
ORMOCER®	0.98	0.96

Peer-reviewed version available at Journal of Sensors and Sensor Systems 2020, 9, 189-197; doi:10.5194/jsss-9-189-2020

shrinkage strain. The comparison area where the fiber freely lies in the matrix is highlighted in gray. The 10 mm in the inlet and outlet area indicates the fiber segments where the fiber was protected from mechanical effects by a tube (Figure 3).

The values illustrate the high correlation between fiber measurement and the reference measurement. Especially with the fiber coating ORMOCER®, the shrinkage strain can be almost completely transferred along the entire measuring length, which indicates a nearly loss-free strain transfer. During the acrylate coating, strain transfer losses were observed in the inlet and outlet areas of the fiber (cf. Figs. 5 and 6); in the center of the specimen, the strain increases to the level of the other two coatings.

The comparison between two measurement times t_1 and t_2 shows strain losses for increasing shrinkage deformation. Although the strain transfer quotient (Table 8) of the acrylate and polyimide fibers decreases by $< 4\%$, the loss in ORMOCER® coating is constant at $< 2\%$.

All specimens were similarly produced and show minor artifacts (Figure 5, O1, O2). Only the ORMOCER® coating shows indicates a loss-free strain transfer compared to the reference measurement and can be used for shrinkage measurement ($t_1 < 2\%$, $t_2 < 4\%$). In the acrylate coating, strain losses were observed in the inlet and outlet areas of the fiber in the specimen, and they indicate a slip between coating and cladding (cf. Figure 1 b). The strains in the middle area of the specimen reached those of the other coating materials. In the case of polyimide and acrylate coatings, small losses ($< 3\%$) were observed between two measurement points during the strain transfer and losses of approximately $8\,\%to10\,\%$ compared to the reference measurement.

4 Discussion

In summary, the test design is well suited for assessing the shrinkage behavior with fiber-optic strain measurements. Furthermore, the usefulness of the DOFS for the measurement of deformations in the matrix of fine-grain concretes is shown. Compared to the data from [25] and [17], all coatings showed significantly lower strain losses. The results indicate that the ORMOCER® coating material can be used for adequate strain measurement in fine-grain concretes. In the case of polyimide coating, small losses of $< 8\%$ were observed. Only for acrylate coating should a strain initiation length of at least 40 mm be provided. The lower stiffness of the material may cause poorer strain transfer in these areas. The acrylate and polyimide coatings showed low losses of $< 3\%$ at time t_2 compared to the measurement after three days. The bond between substrate and coating is assumed to cause the deficits. Except for the entrance area at sample O-2 (Table 3, Figure 5), all specimens were close to each other and only slightly different from the reference measurement. Considering the imprecision of both measuring methods and the fact that the fiber measurement did not cover the whole specimen, the mentioned deviations are negligibly small.

The cause of the artifacts of the samples O1-t_1 and O2-t_1 at positions 20 mm and 150 mm is not clarified. This could be a measurement error or a partially increased

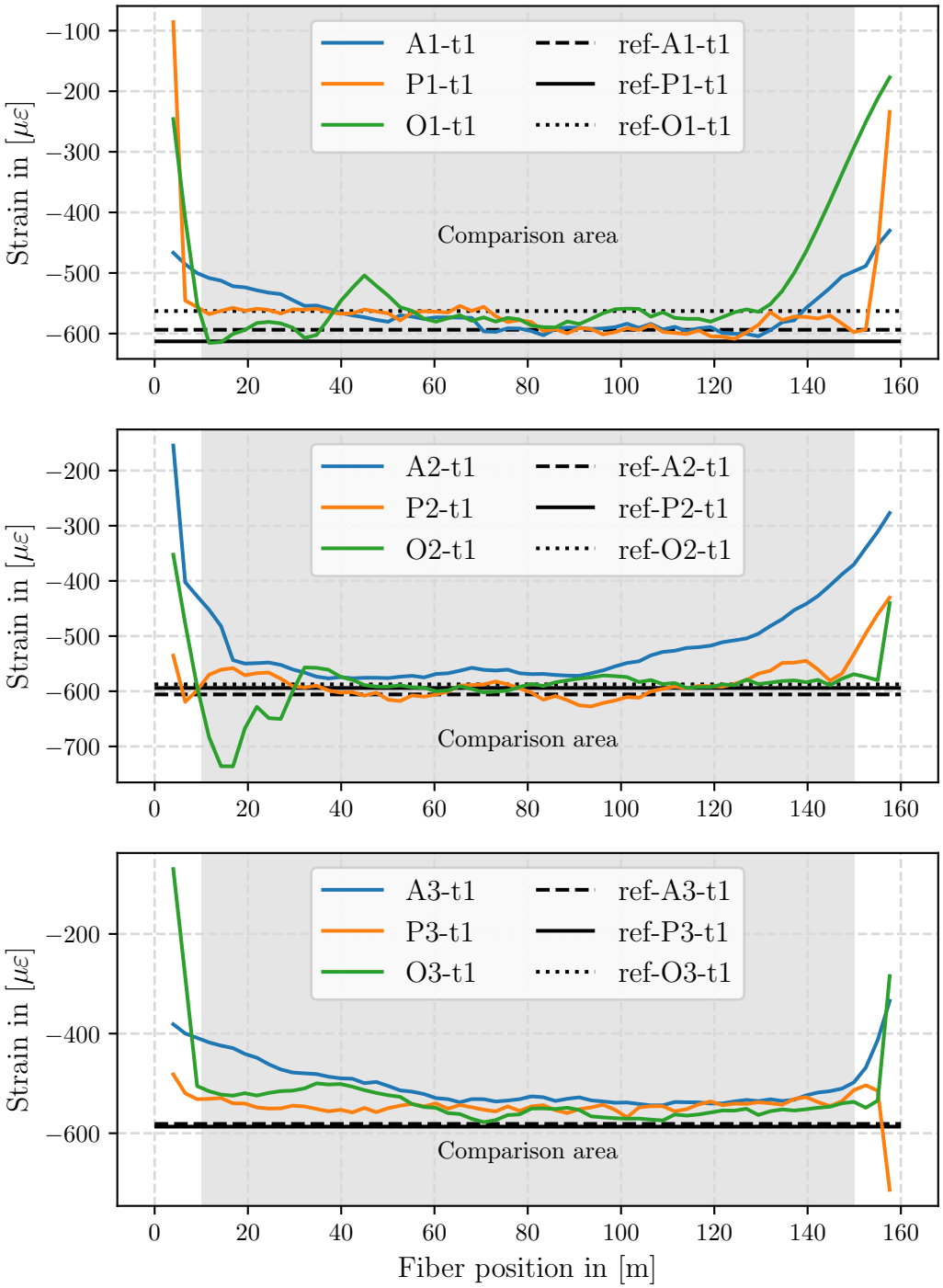

Figure 5: Strain profiles of all specimens at test time t_1

Preprints (www.preprints.org) | NOT PEER-REVIEWED | Posted: 5 March 2020 doi:10.20944/preprints201911.0046.v2

Peer-reviewed version available at Journal of Sensors and Sensor Systems 2020, 9, 189-197; doi:10.5194/jsss-9-189-2020

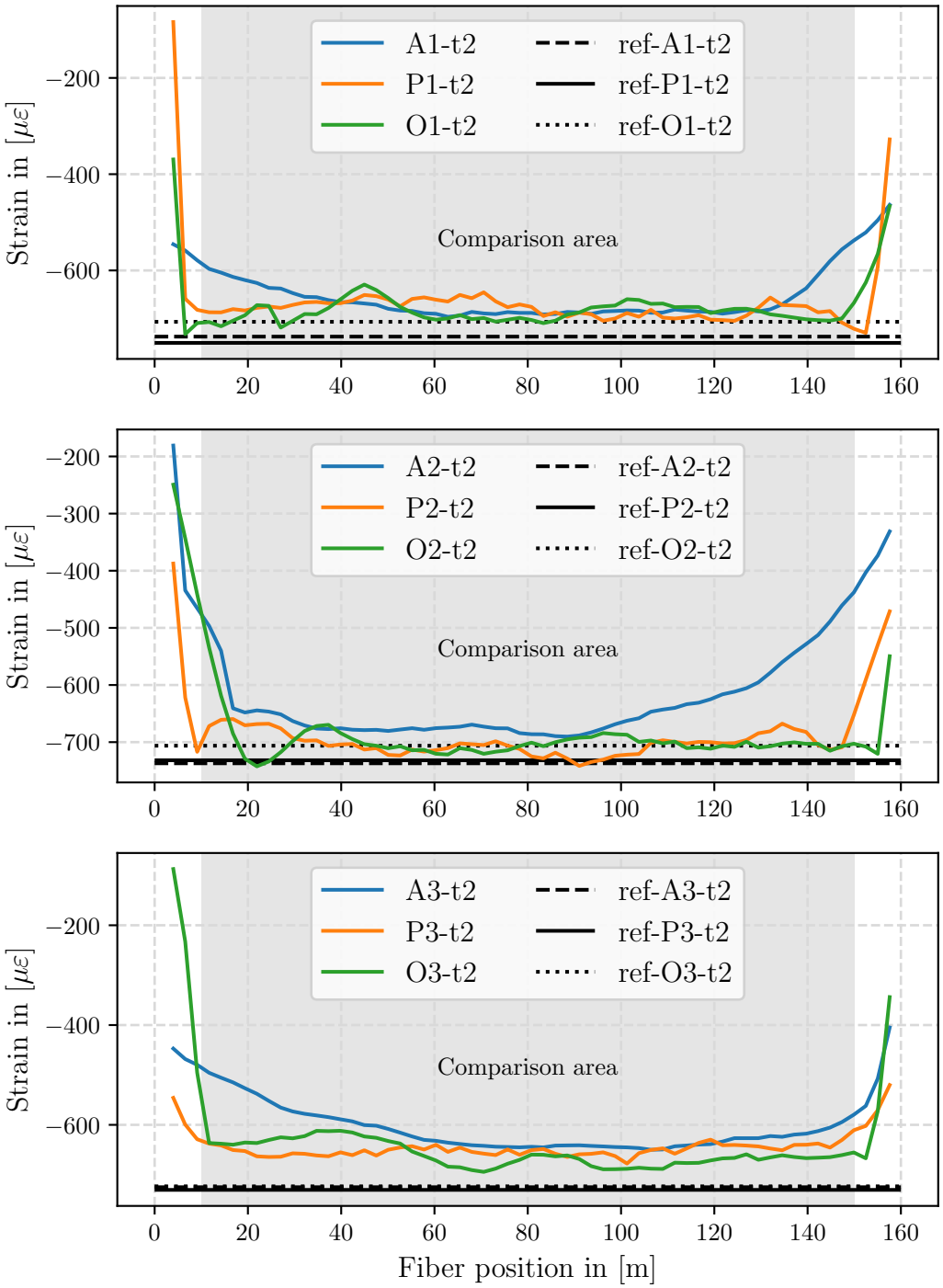

Figure 6: Strain profiles of all specimens at test time t_2

and decreased shrinkage reaction, respectively. Since the anomalies occurred in a reduced form at measurement time t_2, the authors do not assume a measurement error. Further investigations are necessary for this purpose.

The fiber optic sensor technology offers exciting advantages over the established measurement methods for strain measurement in the matrix. With the use of DOFS, the strain can be determined at every point of the fiber, and the sensor fiber can be directly integrated into the concrete structure. Particularly with large concrete components, differences can occur in the shrinkage measurement at the surface compared to that in the matrix. For a strain measurement that corresponds to the real deformation of the component, the strain transfer between substrate and coating and between coating and cladding should be investigated (Figure 1). Only the frequency shift in the fiber core can be used to determine the strain. In addition to the slip relationship, the correct integration of the fiber into the concrete structure is a challenge. The sensor must retain its intended position even after concreting. Another important aspect is the curing time of the fresh concrete. Only when the concrete has sufficiently hardened, the deformations can be transferred to the fiber. In the tests, the measurement was started 24 hours after concreting.

The tests form a basis for the possibilities of the DOFS to measure the strain in the concrete matrix and the SHM of concrete components, especially for precast elements. Besides, the strain transfer properties of the three coating materials for deformation measurements in the matrix are evaluated in more detail. However, further investigations are necessary for SHM: For example, the behavior of the fiber sensor remains unclear regarding the position when larger aggregates are used. Another important aspect is the protection of the fiber against destruction. The moisture, aggregates of the concrete, and paving conditions on the construction site is essential in this respect. Strain cables can help here. However, in contrast to fibers that are exclusively protected by the coating, the larger structure of cables increases the slip-related expansion losses. Furthermore, the long-term stability of the sensors is unclear. In particular, the moist, alkaline milieu of concrete can impair the strain transfer during long-term monitoring. In addition to the investigation of other coating materials and cable types, the behavior of the fiber sensors under mechanical loads will be a future object of investigation. Until now, the measuring method has only been tested under pressure loads for the presented case. The strain transfer behavior under tensile loads and the resulting formation of cracks remain unclear.

5 Conclusion

The investigation compared different coating materials for their strain transfer properties during the strain measurement in the matrix using shrinkage tests. If the represented requirements are fulfilled, exact and reproducible results can be achieved with the ORMOCER® coating material. The following conclusions are drawn from the study:

Peer-reviewed version available at Journal of Sensors and Sensor Systems 2020, 9, 189-197; doi:10.5194/jsss-9-189-2020

- The study shows the successful use of DFOS for strain measurement in the concrete matrix.
- The measured strain losses are lower compared to the literature; therefore, the use of transfer functions is unnecessary.
- The test set-up is suitable for the validation of different fiber coatings regarding their strain transmission rates.
- The exact position of the fiber in the matrix during and after concreting is decisive for the indicated strains.
- The concrete should be sufficiently cured to guarantee the strain transfer. In the tests, the measurement was begun after 24 hours.
- With the ORMOCER® coating, almost no strain losses were detected at the first sampling time.
- In the case of the acrylate and polyimide coatings, an approximately 3% loss occurred between the first and second measurements.
- The acrylate coating showed higher strain losses in the boundary areas than in the middle of the test specimen (max. 37%). From a strain introduction length of approximately 40 mm, the acrylate fiber showed strains at the level of the reference measurement and two other coating materials.
- For the immense amount of data, additional post-processes and error algorithms are necessary to exclude system-related measurement errors and precisely display the results.

Data availability. The datasets used and analyzed in the current study are available from the corresponding author on reasonable request.

Author contributions. MW performed the experiments with the distributed optic sensors, evaluated the data concerning the topic, and wrote the final paper. KH and TB accompanied the experiments and advised on the conceptual design of the paper. All authors read and approved the final paper.

Competing interests. The author declares that they have no conflict of interest.

Acknowledgments. This research is co-financed by tax revenues based on the budget adopted by the members of the Saxon Parliament (promotion reference: K- 7531.20/434-14; SAB no. 100316843). Furthermore, WILEY AUTHOR SERVICES proofread the paper.

Peer-reviewed version available at Journal of Sensors and Sensor Systems 2020, 9, 189-197; doi:10.5194/jsss-9-189-2020

References

[1] Bao, Y. et al. "Distributed fiber optic sensor-enhanced detection and prediction of shrinkage-induced delamination of ultra-high-performance concrete overlay". In: *Smart Materials and Structures* 26.8 (July 2017), p. 085009. DOI: 10.1088/1361-665x/aa71f4.

[2] Bao, Y. et al. "Measuring mortar shrinkage and cracking by pulse pre-pump Brillouin optical time domain analysis with a single optical fiber". In: *Materials Letters* 145 (Apr. 2015), pp. 344–346. DOI: 10.1016/j.matlet.2015.01.140.

[3] Barrias, A. et al. "Application of distributed optical fiber sensors for the health monitoring of two real structures in Barcelona". In: *Structure and Infrastructure Engineering* 14.7 (Feb. 2018), pp. 967–985. DOI: 10.1080/15732479.2018.1438479.

[4] Betz, D. C. et al. "Advanced layout of a fiber Bragg grating strain gauge rosette". In: *Journal of lightwave technology* 24.2 (2006), pp. 1019–1026.

[5] Brault, A. and Hoult, N. "Distributed Reinforcement Strains: Measurement and Application". In: *ACI Structural Journal* 116.4 (July 2019). DOI: 10.14359/51714483.

[6] Cheng, C.-C. et al. "An investigation of bonding-layer characteristics of substrate-bonded fiber Bragg grating". In: *Journal of lightwave technology* 23.11 (2005), p. 3907.

[7] Czarske, J. and Müller, H. "Heterodyne detection technique using stimulated Brillouin scattering and a multimode laser". In: *Optics Letters* 19.19 (Oct. 1994), p. 1589. DOI: 10.1364/ol.19.001589.

[8] Davis, M. B. et al. "Distributed Sensing for Shrinkage and Tension Stiffening Measurement". In: *ACI Structural Journal* 114.3 (May 2017). DOI: 10.14359/51689463.

[9] Delepine-Lesoille, S. et al. "Quasi-distributed optical fibre extensometers for continuous embedding into concrete: design and realization". In: *Smart Materials and Structures* 15.4 (May 2006), pp. 931–938. DOI: 10.1088/0964-1726/15/4/005.

[10] *DIN 52 450:1985-08, Testing of inorganic non-metallic building materials; Determination of shrinking and swelling on small test pieces.* (DIN 52450:1985).

[11] Dyckerhoff GmbH. *C3 Carbon Concrete Composite. Bindemittel für hochfeste Carbonbetone.* Feb. 1, 2017. URL: http://www.dyckerhoff.com/online/de/Home/Unternehmen/ForschungundEntwicklung/Projekte/documento423.html (visited on 09/17/2019).

[12] FBGS International N.V. *DTG coating Ormocer®-T for Temperature Sensing Applications*. Feb. 1, 2015. URL: https://fbgs.com/wp-content/uploads/2019/03/Introducing_and_evaluating_Ormocer-T_for_temperature_sensing_applications.pdf (visited on 09/16/2019).

[13] Fischer, O., Thoma, S., and Crepaz, S. "Quasikontinuierliche faseroptische Dehnungsmessung zur Rissdetektion in Betonkonstruktionen". In: *Beton- und Stahlbetonbau* 114.3 (Jan. 2019), pp. 150–159. DOI: 10.1002/best.201800089.

[14] Froggatt, M. and Moore, J. "High-spatial-resolution distributed strain measurement in optical fiber with Rayleigh scatter". In: *Applied Optics* 37.10 (1998), pp. 1735–1740.

[15] Gifford, D. K. et al. "Distributed fiber-optic temperature sensing using Rayleigh backscatter". In: *2005 31st European Conference on Optical Communication, ECOC 2005*. Vol. 3. IET. 2005, pp. 511–512.

[16] Henault, J. M. et al. "Analysis of the strain transfer mechanism between a truly distributed optical fiber sensor and the surrounding medium". In: *Concrete Repair, Rehabilitation and Retrofitting III*. CRC Press, 2012, pp. 288–289.

[17] Henault, J.-M. et al. "Quantitative strain measurement and crack detection in RC structures using a truly distributed fiber optic sensing system". In: *Construction and Building Materials* 37 (Dec. 2012), pp. 916–923. DOI: 10.1016/j.conbuildmat.2012.05.029.

[18] Henault, J.-M. et al. "Truly Distributed Optical Fiber Sensors for Structural Health Monitoring: From the Telecommunication Optical Fiber Drawling Tower to Water Leakage Detection in Dikes and Concrete Structure Strain Monitoring". In: *Advances in Civil Engineering* 2010 (2010), pp. 1–13. DOI: 10.1155/2010/930796.

[19] Her, S.-C. and Huang, C.-Y. "Effect of Coating on the Strain Transfer of Optical Fiber Sensors". In: *Sensors* 11.7 (July 2011), pp. 6926–6941. DOI: 10.3390/s110706926.

[20] Horiguchi, T. et al. "Development of a distributed sensing technique using Brillouin scattering". In: *Journal of Lightwave Technology* 13.7 (July 1995), pp. 1296–1302. DOI: 10.1109/50.400684.

[21] Inaudi, D. and Glisic, B. "Application of distributed fiber optic sensory for SHM". In: *Proceedings of the ISHMII-2* 1 (2005), pp. 163–169.

[22] Leung, C. K. Y. et al. "Review: optical fiber sensors for civil engineering applications". In: *Materials and Structures* 48.4 (Nov. 2013), pp. 871–906. DOI: 10.1617/s11527-013-0201-7.

[23] Li, H.-N. et al. "Strain Transfer Coefficient Analyses for Embedded Fiber Bragg Grating Sensors in Different Host Materials". In: *Journal of Engineering Mechanics* 135.12 (Dec. 2009), pp. 1343–1353. DOI: 10.1061/(asce)0733-9399(2009)135:12(1343).

[24] Li, Q., Li, G., and Wang, G. "Effect of the plastic coating on strain measurement of concrete by fiber optic sensor". In: *Measurement* 34.3 (Oct. 2003), pp. 215–227. DOI: 10.1016/s0263-2241(03)00052-6.

[25] Li, Q. et al. "Elasto-Plastic Bonding of Embedded Optical Fiber Sensors in Concrete". In: *Journal of Engineering Mechanics* 128.4 (Apr. 2002), pp. 471–478. DOI: 10.1061/(asce)0733-9399(2002)128:4(471).

[26] López-Higuera, J. M. et al. "Fiber optic sensors in structural health monitoring". In: *Journal of lightwave technology* 29.4 (2011), pp. 587–608.

[27] Ohno, H. et al. "Industrial Applications of the BOTDR Optical Fiber Strain Sensor". In: *Optical Fiber Technology* 7.1 (Jan. 2001), pp. 45–64. DOI: 10.1006/ofte.2000.0344.

[28] Parker, T. R. et al. "A fully distributed simultaneous strain and temperature sensor using spontaneous Brillouin backscatter". In: *IEEE Photonics Technology Letters* 9.7 (July 1997), pp. 979–981. DOI: 10.1109/68.593372.

[29] Samiec, D. "Distributed fibre-optic temperature and strain measurement with extremely high spatial resolution". In: *Photonic International* 6 (2012), pp. 10–13.

[30] Song, K. Y. et al. "Time-Domain Distributed Fiber Sensor With 1 cm Spatial Resolution Based on Brillouin Dynamic Grating". In: *Journal of Lightwave Technology* 28.14 (July 2010), pp. 2062–2067. DOI: 10.1109/jlt.2010.2050763.

[31] Speck, K. et al. "Faseroptische Sensoren zur kontinuierlichen Dehnungsmessung im Beton". In: *Beton- und Stahlbetonbau* 114.3 (Jan. 2019), pp. 160–167. DOI: 10.1002/best.201800105.

[32] Udd, E. *Fiber optic sensors: an introduction for engineers and scientists*. Wiley-Blackwell, Aug. 5, 2011. 512 pp. ISBN: 0470126841. URL: https://www.ebook.de/de/product/13230722/eric_udd_fiber_optic_sensors.html.

[33] Ueberhuber, C. W. *Numerical Computation 1*. Springer Berlin Heidelberg, Feb. 27, 1997. 496 pp. ISBN: 3540620583. URL: https://www.ebook.de/de/product/14678306/christoph_w_ueberhuber_numerical_computation_1.html.

[34] Wan, K. T., Leung, C. K. Y., and Olson, N. G. "Investigation of the strain transfer for surface-attached optical fiber strain sensors". In: *Smart Materials and Structures* 17.3 (2008), p. 035037.

[35] Weisbrich, M. and Holschemacher, K. "Comparison between different fiber coatings and adhesives on steel surfaces for distributed optical strain measurements based on Rayleigh backscattering". In: *Journal of Sensors and Sensor Systems* 7.2 (Nov. 2018), pp. 601–608. DOI: 10.5194/jsss-7-601-2018.

[36] Weisbrich, M., Holschemacher, K., and Kaeseberg, S. "Comparison between different Fiber Optical Strain Measurement Systems Based on the Example of Reinforcing Bars". In: *Procedia Engineering* 172 (2017), pp. 1235–1242. DOI: 10.1016/j.proeng.2017.02.145.

[37] Zeng, X. et al. "Strain measurement in a concrete beam by use of the Brillouin-scattering-based distributed fiber sensor with single-mode fibers embedded in glass fiber reinforced polymer rods and bonded to steel reinforcing bars". In: *Applied Optics* 41.24 (Aug. 2002), p. 5105. DOI: 10.1364/ao.41.005105.